Available online at www.sciencedirect.com

ScienceDirect

www.elsevier.com/locate/jes

JES JOURNAL OF ENVIRONMENTAL SCIENCES

www.jesc.ac.cn

Synergistic effects of Cu species and acidity of Cu-ZSM-5 on catalytic performance for selective catalytic oxidation of *n*-butylamine

Xin Xing[1,2], *Na Li*[1,2], *Jie Cheng*[2,*], *Yonggang Sun*[1,2], *Zhongshen Zhang*[2], *Xin Zhang*[2], *Zhengping Hao*[1,2]

[1] *Key Laboratory of Environmental Nanotechnology and Health Effects, Research Center for Eco-Environmental Sciences, Chinese Academy of Sciences, Beijing 100085, China*

[2] *National Engineering Laboratory for VOCs Pollution Control Material & Technology, Research Center for Environmental Material and Pollution Control Technology, University of Chinese Academy of Sciences, Beijing 101408, China*

ARTICLE INFO

Article history:
Received 12 December 2019
Revised 14 March 2020
Accepted 15 March 2020
Available online 6 May 2020

Keywords:
$CH_3CH_2CH_2CH_2NH_2$
Selective oxidation
Cu-ZSM-5
Cu species
Acid sites

ABSTRACT

In this work, a series of Cu-ZSM-5 catalysts with different SiO_2/Al_2O_3 ratios (25, 50, 100 and 200) were synthesized and investigated in *n*-butylamine catalytic degradation. The *n*-butylamine can be completely catalytic degradation at 350°C over all Cu-ZSM-5 catalysts. Moreover, Cu-ZSM-5 (25) exhibited the highest selectivity to N_2, exceeding 90% at 350°C. These samples were investigated in detail by several characterizations to illuminate the dependence of the catalytic performance on redox properties, Cu species, and acidity. The characterization results proved that the redox properties and chemisorption oxygen primarily affect *n*-butylamine conversion. N_2 selectivity was impacted by the Brønsted acidity and the isolated Cu^{2+} species. Meanwhile, the surface acid sites over Cu-ZSM-5 catalysts could influence the formation of Cu species. Furthermore, *in situ* diffuse reflectance infrared Fourier transform spectra was adopted to explore the reaction mechanism. The Cu-ZSM-5 catalysts are the most prospective catalysts for nitrogen-containing volatile organic compounds removal, and the results in this study could provide new insights into catalysts design for VOC catalytic oxidation.

Introduction

Nitrogen-containing volatile organic compounds (NVOCs), such as *n*-butylamine, trimethylamine, N,N-dimethylformamide, nitrobenzene and acrylonitrile, are representative pollutants that are emitted primarily from pharmaceutical, petrochemical and coating industries (Feng et al., 2020a; He et al., 2019; Huang et al., 2014; Jian et al. 2019; Liotta., 2010; Scirè and Liotta, 2012; Tian et al., 2019). *n*-Butylamine has been extensively used as an ingredient in the manufacture of pesticides (such as thiocarbazides), pharmaceuticals, and emulsifiers (Ma et al., 2018a). Currently, many different VOCs treatment methods have appeared, including incineration, condensation, biological degradation, adsorption, and catalysis oxidation (Everaert and Baeyens, 2004; Feng et al., 2020b; Guieysse et al., 2008; Jiang et al., 2018, 2019; Li et al., 2009; Liu et al., 2016a; Parmar and Rao, 2008). A promising method is selective catalytic oxidation of NVOCs, which can completely eliminate NVOCs at lower temperature

* Corresponding author.
E-mail: jiecheng@ucas.ac.cn (J. Cheng).

https://doi.org/10.1016/j.jes.2020.03.015

with N_2 selectivity was higher than that of direct incineration (Zhang et al., 2016a).

In past decades, noble metal catalysts have been investigated for NVOCs catalytic degradation due to the high activity and lower reaction temperature of these samples (Nanba et al., 2004, 2008). Ma et al. (2018a, 2020) reported that Pd-confined materials were efficient catalysts for *n*-butylamine destruction and explored their structure-activity relationship and reaction mechanism. Moreover, transition metals oxide catalysts were also discussed and showed excellent performance for NVOCs catalytic oxidation (Nanba et al., 2005, 2007). Huang et al. (2010) prepared the structure-activity relationship of CrCe loading on pillared interlayered clays catalysts for *n*-butylamine catalytic oxidation and pointed out that acidity is important in *n*-butylamine oxidation.

In our previous study (Xing et al., 2020), we investigated and discussed the influence of the different topological structures of supports on the performance of Cu-loaded zeolite for *n*-butylamine selective oxidation. It was found that Cu-ZSM-5 catalysts show good catalytic performance in *n*-butylamine catalytic oxidation, their excellent activity depends strongly on the isolated Cu^{2+} species and the acidity of zeolites. The present work is to discuss the mechanism and effects of SiO_2/Al_2O_3 ratio of ZSM-5 supports on the existence form of Cu species and catalytic performance. Hence, we studied the copper species on the zeolite supports and how factors such as physicochemical properties of the support (acidity, SiO_2/Al_2O_3 ratio) influence their formation and redox properties.

1. Materials and methods

1.1. Catalysts synthesis and characterization

The synthesis of catalysts and the characterization of the samples by different technologies with details are shown in Appendix A. Supplementary data.

1.2. Catalytic test

The catalytic performance tests of *n*-butylamine selective oxidation was carried out with the gas flow of 375 ppmV *n*-butylamine, 5 vol.% O_2 and He (balance) in a fixed-bed reactor. About 0.5 mL catalysts were packed in the reactor, which has been pressed and sieved to 40–60 mesh. The gas hourly space velocity (GHSV) of *n*-butylamine selective oxidation can reach approximately 12,000 hr^{-1}. Gas chromatograph (7890A, Agilent, USA) and Fourier transform infrared reflectance (FTIR) gas analyzer (Multi-Gas 2030, MKS, USA) were used for the detection of the effluent gases. Catalytic performance was calculated on the basis of *n*-butylamine conversion and products (N_2, NO, and N_2O) selectivity:

$$n\text{-Butylamine conversion} = \frac{n\text{-Butylamine(in)} - n\text{-Butylamine(out)}}{n\text{-Butylamine(in)}} \times 100\% \quad (1)$$

$$CO/CO_2 \text{ selectivity} = \frac{CO/CO_2}{\text{Total product C}} \times 100\% \quad (2)$$

$$NO/N_2O/N_2 \text{ selectivity} = \frac{NO/N_2O/N_2}{\text{Total product N}} \times 100\% \quad (3)$$

where *n*-Butylamine(in) and *n*-Butylamine(out) are concentrations of *n*-butylamine at the inlet and outlet of reaction pipe, respectively.

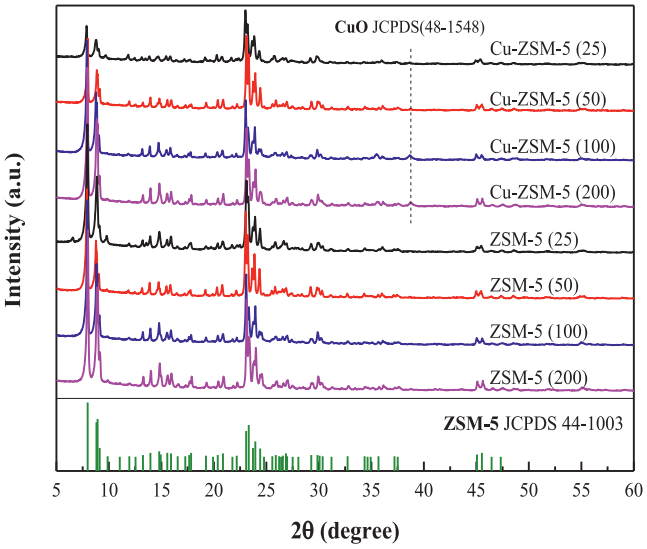

Fig. 1 – X-ray diffraction (XRD) results of pure ZSM-5 and Cu-ZSM-5 with different SiO_2/Al_2O_3 ratios *X* (ZSM-5(X) and Cu-ZSM-5(X)).

2. Results and discussion

2.1. XRD and HR-TEM

The X-ray diffraction (XRD) results of Cu-loaded zeolite samples and their supports are illustrated in Fig. 1. The peaks at $2\theta = 7.9°$, 8.8°, 14.8°, 23.1°, and 23.8° were exhibited, which represented to the (011), (020), (031), (051) and (033) planes of ZSM-5, respectively (Lai et al., 2015; Navlani-García et al., 2015). The obtained curves are well matched with ZSM-5 (JCPDS 44-1003). Comparing with the pure ZSM-5, the XRD patterns of Cu-loaded zeolite samples were not significantly changed, which indicated that the structure of ZSM-5 still maintained after adding of Cu. The peaks of CuO are not obviously occurred for the Cu-ZSM-5 (25), which indicated that the dispersion of Cu species in zeolite support are very high or the aggregated CuO are too small to be detected (Nanba et al., 2004). But the CuO peaks are detected over other samples, and the peak intensity of CuO species increased as the increasing of the ratio of SiO_2 and Al_2O_3, which demonstrated that the dispersion of CuO of Cu-ZSM-5 with high SiO_2/Al_2O_3 was lower than the catalysts with low SiO_2/Al_2O_3. The average diameter of CuO particles over Cu-ZSM-5 catalysts were obtained from High-resolution transmission electron microscopy (HR-TEM) images (Fig. 2), which was 3.1–3.9 nm and the CuO particles highly dispersed on all catalysts. Similarly, the CuO particles average size increased slightly with the increasing of SiO_2/Al_2O_3, which corresponded to the results of XRD.

2.2. Catalytic performance

Fig. 3a shows the *n*-butylamine conversion over Cu-loaded zeolite samples, and the temperatures at 50%, 90%, and 100% conversion (T_{50}, T_{90}, T_{100}) and N_2 selectivity values are listed in Table 1. The *n*-butylamine conversion over all samples increased with increasing the reaction temperature. Cu-ZSM-5(100) sample presented the highest conversion of *n*-butylamine selective oxidation in the entire temperature range, and *n*-butylamine was achieved almost complete conversion at 300°C. The T_{50} decreased in the order of Cu-ZSM-5

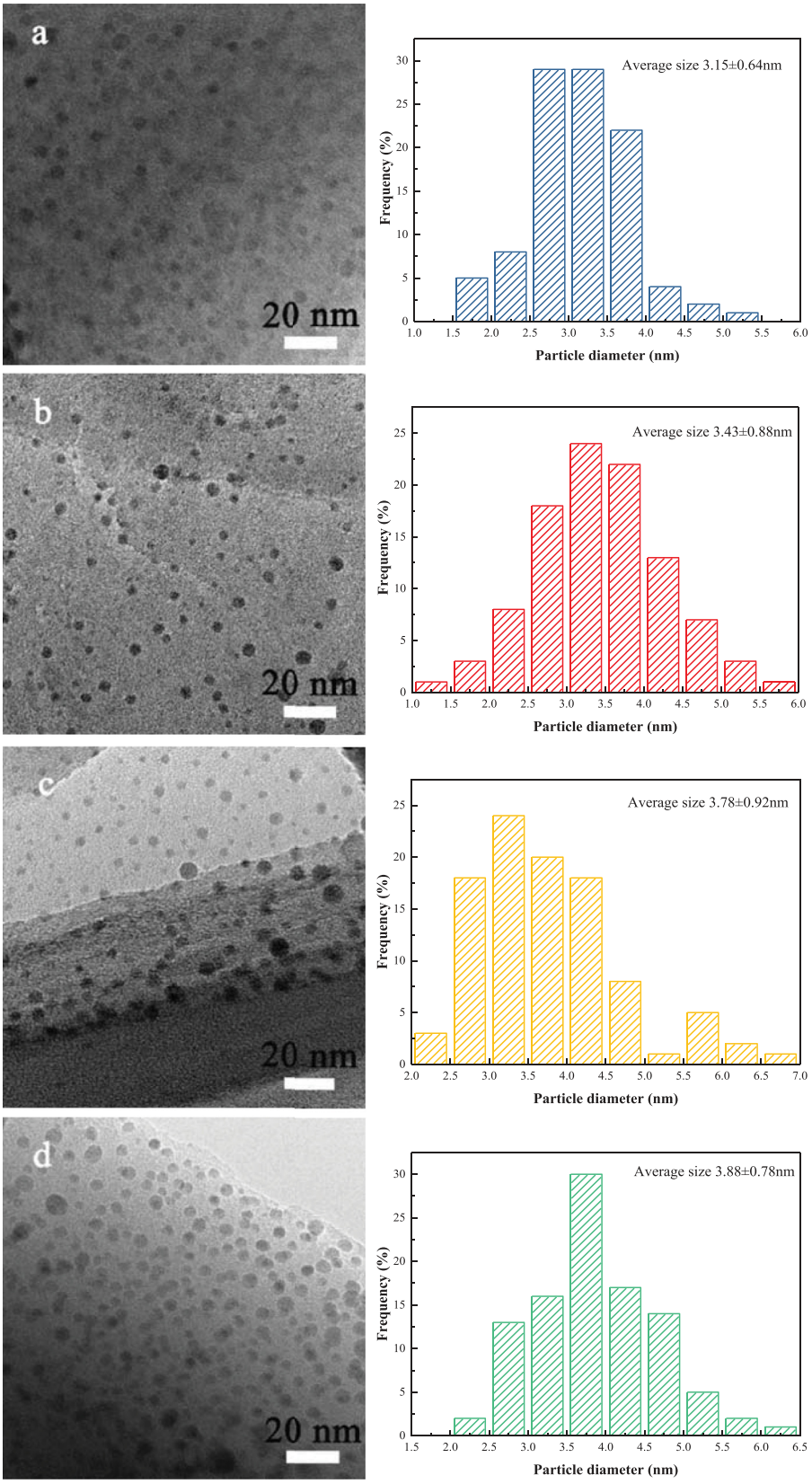

Fig. 2 – High-resolution transmission electron microscopy (HR-TEM) images and particle diameter distributions of Cu-ZSM-5 catalysts with different SiO_2/Al_2O_3 ratios (a) 25, (b) 50, (c) 100, and (d) 200.

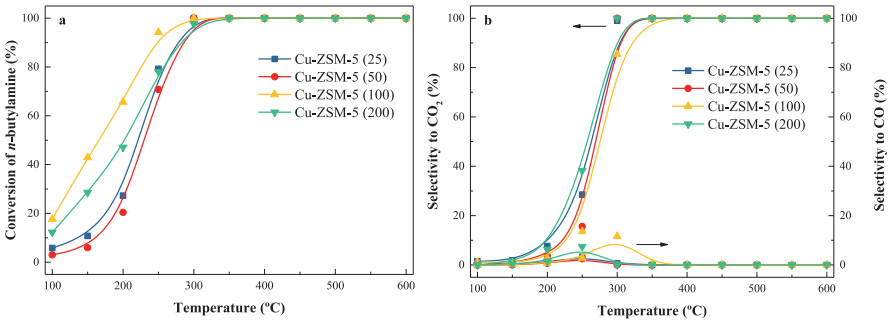

Fig. 3 – (a) *n*-Butylamine conversion of Cu-ZSM-5 and (b) the selectivity to CO_2 and CO over Cu-ZSM-5 catalysts.

Table 1 – Temperatures at 50%, 90%, and 100% conversion (T_{50}, T_{90}, T_{100}) and N_2 selectivity of Cu-ZSM-5 catalysts.

Sample	T_{50} (°C)	T_{90} (°C)	T_{100} (°C)	N_2 selectivity (%)		
				350°C	400°C	450°C
Cu-ZSM-5 (25)	223	267	300	92.46	95.27	97.14
Cu-ZSM-5 (50)	230	274	300	90.70	94.28	94.13
Cu-ZSM-5 (100)	165	239	300	88.72	84.00	74.37
Cu-ZSM-5 (200)	207	275	350	69.06	59.89	52.91

(50) > Cu-ZSM-5 (25) > Cu-ZSM-5 (200) > Cu-ZSM-5 (100). However, the T_{100} of Cu-ZSM-5 (200) was 350°C, which was higher than that of other samples. Furthermore, the selectivity to CO_2 and CO is shown in Fig. 3b. Minimal CO_2 and CO were produced below 200°C, indicating that *n*-butylamine was oxidized to organic byproducts instead of to CO_2 and CO at the initial of reaction. The CO_2 selectivity increased with the increasing of temperature, reaching 100% at 300–350°C. However, the selectivity to CO first increased and subsequently decreased near 250°C, and no CO was produced at 300–350°C. Interestingly, although Cu-ZSM-5 (100) presented the excellent conversion of *n*-butylamine, the formation of CO_2 was lower and that of CO was higher than other samples.

As mentioned in the introduction, we focus attention on the nitrogen-containing products ($NO/N_2O/N_2$) in *n*-butylamine selective catalytic oxidation. The N_2O, N_2, and NO selectivity over Cu-loaded zeolite catalysts are displayed in Fig. 4. At low temperature (below 350°C), the major nitrogen-containing product was N_2O and N_2. For the formation of N_2O, the N_2O selectivity first increased as temperature increased, peaked at 350°C and disappeared at 450°C. Notably, the N_2O selectivity over Cu-ZSM-5 (25) was greater than that of other samples at the low temperature range (150–250°C), but Cu-ZSM-5 (200) produced more N_2O at 350–500°C. The N_2 selectivity decreased in the following order: Cu-ZSM-5 (25) > Cu-ZSM-5 (50) > Cu-ZSM-5 (100) > Cu-ZSM-5 (200). Nitrogen was minimally generated below 200°C, then N_2 selectivity increased rapidly, reached a peak value and decreased with temperature increasing. The N_2 selectivity began to decline at above 350°C over Cu-ZSM-5 (100) and Cu-ZSM-5 (200) catalysts, but the values of Cu-ZSM-5 (25) and Cu-ZSM-5 (50) were still increased, reaching more than 95% at 450°C, and subsequently decreased as the temperature increased. High temperature led to a reduction of N_2 selectivity. For Cu-ZSM-5 (200) catalyst, N_2 selectivity was less than 30% at 600°C, which could be attributed to the formation of NO. According to the temperature, the NO selectivity could be divided into two stages. In 100–350°C, NO selectivity first increased and then decreased. Few NO_x was generated at 350°C for Cu-ZSM-5 (25) and Cu-ZSM-5 (50). Moreover, when the reaction temperature of *n*-butylamine selective oxidation was above 350°C, the selectivity to NO increased obviously. Moreover, no NO_2 was generated during the whole reaction process over Cu-loaded zeolite samples.

In summary, Cu-ZSM-5 (100) showed the high conversion rate, but the N_2 selectivity of this catalyst was less than satisfactory, reaching 88% at 350°C and decreasing to 44% at 600°C. For Cu-ZSM-5 (25), its initial conversion was lower than Cu-ZSM-5 (100), but the T_{100} is same as that of Cu-ZSM-5 (100). Additionally, the N_2 selectivity of Cu-ZSM-5 (25) was the highest among all samples, exceeding 95% at 400–450°C. Even at higher temperature, the formation of NO increased, and N_2 selectivity was still 75% at 600°C.

2.3. *H_2-TPR results*

H_2 temperature-programmed reduction (H_2-TPR) results of Cu-ZSM-5 samples are exhibited in Fig. 5. Two or three H_2 reduction peaks appeared over Cu-ZSM-5 catalysts. The peaks at low temperature (226, 294, 243, 332 and 310°C) corresponded to the reduction of CuO nanoparticles, which are highly dispersed on the surface of supports, including isolated Cu^{2+} and surface CuO cluster species. The reduction peak at 226°C of Cu-ZSM-5 (25) probably ascribed to the isolated Cu^{2+}, and another peak at 294°C could be assigned to the oligomers of Cu-O-Cu species (Liu et al., 2016b). The peaks at high temperature (375, 317, 434 and 386°C) were attributed to the bulk CuO species (Xue et al., 2018). Additionally, we calculated the consumption of H_2 of different peaks over four catalysts based on the peak area (Table 2). The total consumption of H_2 of all samples decreased in the order that Cu-ZSM-5 (100) > Cu-ZSM-5 (50) > Cu-ZSM-5 (25) > Cu-ZSM-5 (200), Cu-ZSM-5 (100) has the highest H_2 consumption, reached 0.565 mmol/g, but the H_2 consumption of Cu-ZSM-5 (200) was 0.415 mmol/g, which demonstrated that the redox abilities were weaker than those of other samples. Notably, the H_2 consumption of lower temperature peak decreased in the following order: Cu-ZSM-5 (100) > Cu-ZSM-5 (200) > Cu-ZSM-5 (25) > Cu-ZSM-5 (50), which suggested that low-temperature activity might be poor over Cu-ZSM-5 (50).

Combined with the catalytic performance, the T_{50} value occurred in the following order: Cu-ZSM-5 (100) < Cu-ZSM-5 (200) < Cu-ZSM-5 (25) < Cu-ZSM-5 (50). The results are in accordance with decreasing order of H_2 consumption at lower temperature. It demonstrated that the H_2 consumption of low temperature impacts the low temperature conversion of *n*-butylamine. Hence, Cu-ZSM-5 (100) and Cu-ZSM-5 (200) samples has good low temperature activity. The total conversion temperature of *n*-butylamine over Cu-ZSM-5 (200) sample was 350°C, which was the highest among all samples. It could be ascribed to the poor redox properties of Cu-ZSM-5 (200), because the H_2 consumption of this sample was the lowest. To summarize, the redox properties are one of the vital factors which influence the *n*-butylamine catalytic oxidation.

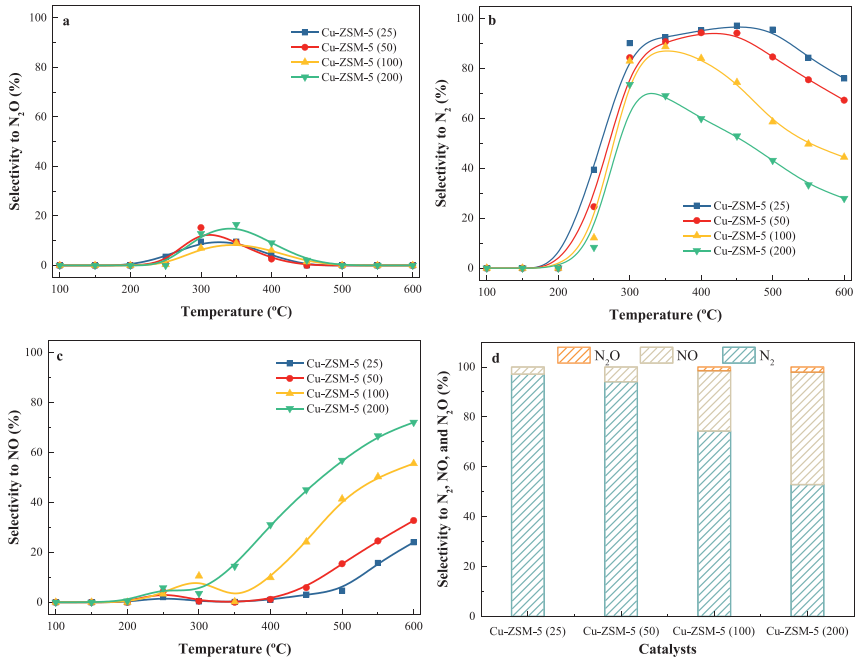

Fig. 4 – (a) N_2O, (b) N_2, (c) NO selectivity and (d) product selectivity at 450°C over Cu-ZSM-5 catalysts.

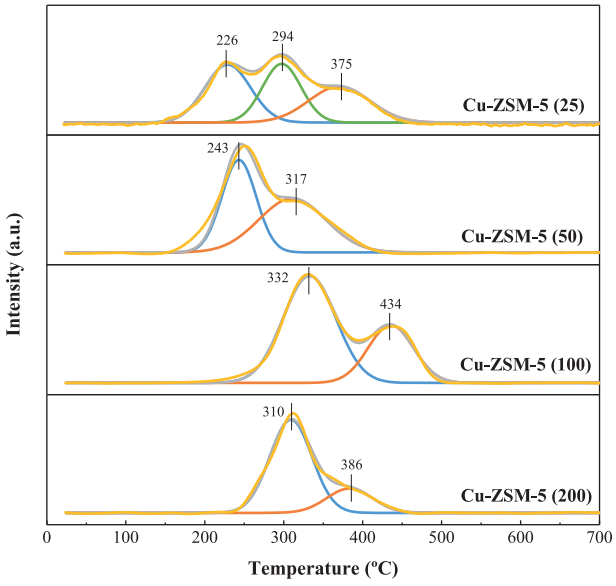

Fig. 5 – H_2 temperature-programmed reduction (H_2-TPR) results of Cu-ZSM-5 catalysts.

Table 2 – H_2 consumption of the Cu-ZSM-5 catalysts.

Sample	Peak position (°C)	H_2 consumption (mmol/g)	Total H_2 consumption (mmol/g)
Cu-ZSM-5(25)	226	0.199	0.477
	294	0.126	
	375	0.152	
Cu-ZSM-5(50)	243	0.225	0.482
	317	0.257	
Cu-ZSM-5(100)	332	0.401	0.565
	434	0.164	
Cu-ZSM-5(200)	310	0.336	0.415
	386	0.079	

2.4. *Characterizations of Cu species (XPS, EPR, and UV–Vis)*

2.4.1. *XPS results*

The surface chemical state of Cu-ZSM-5 samples was obtained from X-ray photoelectron spectra (XPS) analysis (Fig. 6), and Table 3 lists the surface atom concentrations of these catalysts. The Cu 2p XPS spectra for different SiO_2/Al_2O_3 Cu-ZSM-5 are displayed in Fig. 6a. The shake-up satellite feature centered at binding energies near 944.5 and 964.0 eV, which are characteristics of Cu, is predominantly present on the surface as Cu^{2+}. Two main peaks appeared at 935.1 eV and 954.5 eV, which could be ascribed to Cu2p3/2 and Cu2p1/2 (Lai et al., 2015). Moreover, the peaks of Cu2p3/2 could be divided into two peaks. The peak at around 934.3 eV represented to the agglomerated CuO species, and the peak located at 935.8 eV could be due to isolated Cu^{2+} ion in octahedral coordination (Pereda-Ayo et al., 2014). Interestingly, the amount of Cu impregnation was 5% for all catalysts, but the Cu contents of the surface was far below 5% (Table 3). The surface atomic ratio of Cu over Cu-ZSM-5 (25) surface was 2.15%, a maximum among all samples, indicating the presence of highly dispersed Cu species, which was consistent with the XRD results. Additionally, the proportion of isolated Cu^{2+} and (isolated Cu^{2+} + CuO) was 0.73 over Cu-ZSM-5 (25), denoting that there are more isolated Cu^{2+} exists on Cu-ZSM-5 (25) surface. The decreased order of isolated Cu^{2+}/ (isolated Cu^{2+} + CuO) is agreement with the decreased order of N_2 selectivity in *n*-butylamine selective oxidation.

The XPS spectra of O1s for Cu-loaded zeolite samples are shown in Fig. 6b. The main peaks occurred at around 530.4 eV, which corresponded to the lattice oxygen species (O_{latt}) of catalysts. The shoulder peaks at 531.5 eV ascribed to the chemisorbed oxygen species (O_{ads}), which could be attributed to the hydroxyl groups (Sun et al., 2017). According to literature, the O_{ads} is necessary for catalytic oxidation reaction because of the higher mobility (Lian et al., 2014). Herein, we

Table 3 – Surface atom concentrations of Cu-ZSM-5 samples.

Sample	$O_{ads}/(O_{ads} + O_{latt})$	Isolated Cu^{2+}/(Isolated Cu^{2+} + CuO)	Surface composition (%)			
			Cu	Si	Al	O
Cu-ZSM-5 (25)	0.69	0.73	2.15	28.65	9.44	59.76
Cu-ZSM-5 (50)	0.67	0.56	1.78	30.91	7.58	59.73
Cu-ZSM-5 (100)	0.76	0.52	0.73	32.41	3.75	63.11
Cu-ZSM-5 (200)	0.73	0.48	1.69	31.54	6.40	60.37

Surface composition: atomic ratio on surface.

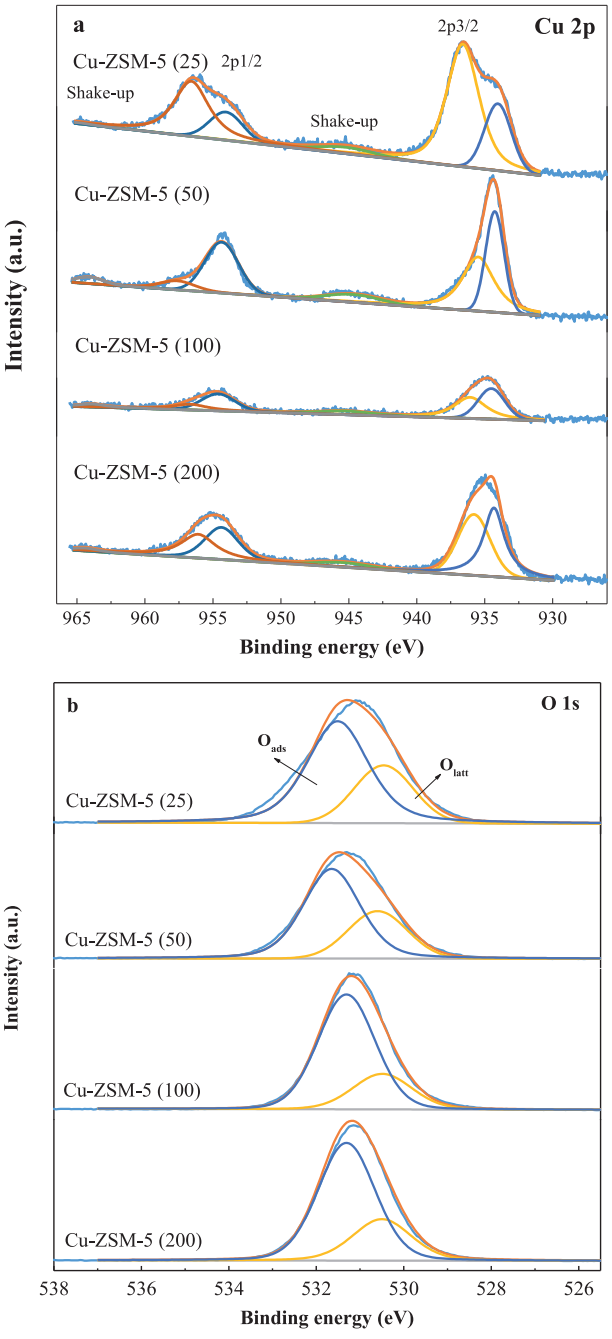

Fig. 6 – X-ray photoelectron spectra (XPS) spectra of (a) Cu2p and (b) O1s of Cu-ZSM-5 catalysts. O_{ads}: chemisorbed oxygen species; O_{latt}: lattice oxygen species.

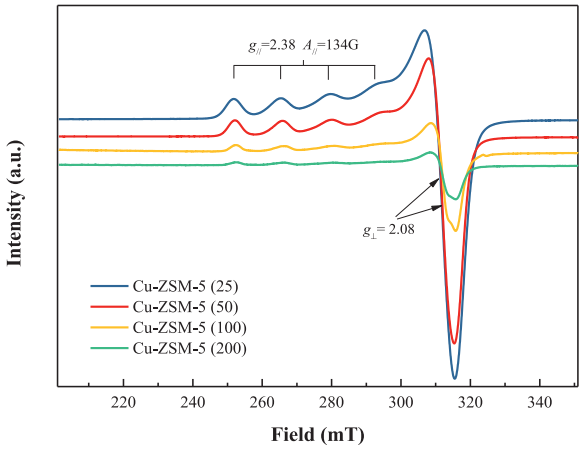

Fig. 7 – Electron paramagnetic resonance (EPR) spectra of Cu-ZSM-5 catalysts.

calculated the proportion of O_{ads} and (O_{ads} + O_{latt}) (Table 3). The O_{ads} and (O_{ads} + O_{latt}) proportion values decreased in the following order: Cu-ZSM-5 (100) > Cu-ZSM-5 (200) > Cu-ZSM-5 (25) > Cu-ZSM-5 (50). The sequence corresponds to the decrease order of low temperature hydrogen consumption. The O_{ads} and (O_{ads} + O_{latt}) proportion values over Cu-ZSM-5 (100) (0.76) is relatively higher among all the samples, indicating the existence of more O_{ads}, and this oxygen species is also an important factor for the conversion of *n*-butylamine, especially at low temperature.

2.4.2. *EPR results*

Electron paramagnetic resonance (EPR) is highly sensitive to the ligand geometry of paramagnetic transition metal ions, and isolated Cu^{2+} species give a strong EPR response that could be detected at both low temperature and at room temperature. Fig. 7 presents the EPR spectrum of Cu-loaded zeolite samples. The EPR spectra shows that all the samples had isolated Cu^{2+} species with a resolved hyperfine structure of g factors with $g_{//} = 2.38$, $A_{//} = 134$ G, and $g_{\perp} = 2.08$, which usually corresponded to the isolated Cu^{2+} species with tetragonally distorted octahedral coordination (Yashnik et al., 2005). According to the literature, the isolated Cu^{2+} species are usually existed in ion exchange sites of ZSM-5 supports (Yashnik et al., 2012). The EPR results show that the higher of SiO_2/Al_2O_3 ratio, the less isolated Cu^{2+} species. This result indicates that the increase of the ratio of SiO_2 and Al_2O_3 ratio will decrease the ion exchange positions of supports. Therefore, the isolated Cu^{2+} species on the catalyst with high SiO_2/Al_2O_3 ratio will be reduced. In addition, with the increase of the proportion of SiO_2 and Al_2O_3, the spectra are observed to broaden with less defined hyperfine splitting, and it indicates that the interactions between neighboring Cu^{2+} ions got stronger. The decrease of peak intensity of isolated Cu^{2+} species and the sig-

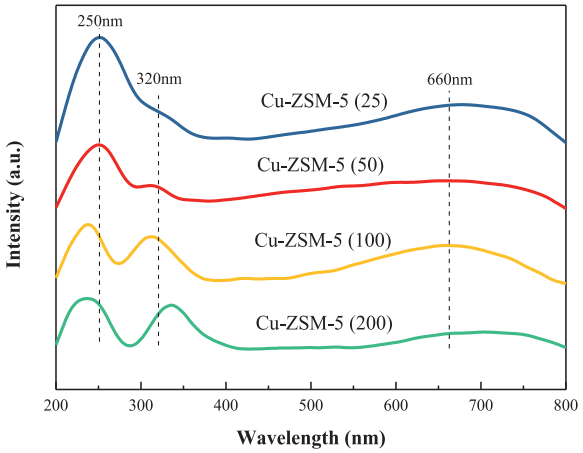

Fig. 8 – UV–Vis diffuse reflectance spectra (UV–Vis DRs) of Cu-ZSM-5 catalysts.

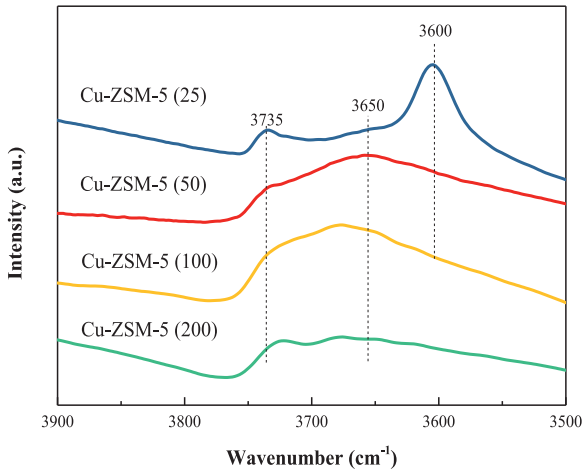

Fig. 9 – Hydroxyl groups of the infrared (IR) spectra of Cu-ZSM-5 measured at 100°C.

nal broadening might result from an increase in aggregated oligomeric Cu-O-Cu species. This result is consistent with the UV–Vis-DRs analysis result.

2.4.3. *UV–Vis-DRs*

The coordination mode of Cu species was studied via UV–Vis diffuse reflectance spectra (UV–Vis DRs), are shown in Fig. 8. The spectra were divided into three regions, the strong band at 250 nm could be attributed to the charge transfer from the molecular orbital of ligand to metal, mainly from the orbital of O^{2-} to that of isolated Cu^{2+}, implying that certain Cu^{2+} ions are embraced into ZSM-5 framework. In addition, absorption peak appearing at approximately 320 nm is also a charge transfer band (LMCT, $O^{2-} \rightarrow Cu^{2+}$), which is characteristic of the oligomeric Cu^{2+}-O^{2-}-Cu^{2+} chain, such as cluster CuO species (Xing et al., 2019). The low intensity band at 600–800 nm is observed in the visible or the near infrared ranges and is attributed to the d-d transition of Cu^{2+}. According to the literature, the green color of the materials is the results of this d-d transition (Das et al., 2012; Praliaud et al. 1998; Rutkowska et al., 2017). Based on the results, it could be confirmed that Cu species in Cu-loaded zeolite samples are presented in different environments: isolated Cu^{2+} species exchanged on the framework of ZSM-5, and the oligomeric Cu^{2+}-O^{2-}-Cu^{2+} chain or CuO particles forms dispersed on the zeolite surface. Notably, the proportion of SiO_2 and Al_2O_3 impacted the distribution of isolated Cu^{2+} and cluster CuO. The intensity of oligomeric Cu^{2+}-O^{2-}-Cu^{2+} increased with increasing of the proportion of SiO_2 and Al_2O_3.

According to the results of XPS, EPR, and UV–Vis-DRs results, with the increase of the proportion of SiO_2 and Al_2O_3, the isolated Cu^{2+} species significantly decreased, which is in accordance with the decreasing order of N_2 selectivity. In the previous study, we suggested that isolated Cu^{2+} species may be an important factor to restrict the formation of N_2. In this work, we further confirmed that the isolated Cu^{2+} species are critical for *n*-butylamine selective oxidation to N_2.

2.5. *Characterization of acidity*

2.5.1. *IR spectra of hydroxyl groups*

Fourier transform infrared (FTIR) spectroscopy was carried out to characterize the hydroxyl groups, as shown in Fig. 9. The hydroxyl groups of the infrared spectra (IR) of Cu-ZSM-5 (25) consisted of two bands. The band near 3735 cm^{-1} could be due to the existence of terminal silanol groups over Cu-loaded zeolite samples, and the absorption peak centered at 3600 cm^{-1} is corresponded to the bridging hydroxyl groups (Brønsted acidity). Furthermore, the broad peak at 3650 cm^{-1} could be ascribed to OH groups adjacent to extra-framework aluminum species (Ma et al., 2018b). For other samples, the peaks of 3735 and 3600 cm^{-1} were not obvious, especially the peak of 3600 cm^{-1}. As stated in the literature, the peak at 3600 cm^{-1} is connected with the Brønsted acidic, which corresponded to the vibration of bridging hydroxyl in channels or cages, indicated that the Brønsted acidity of Cu-ZSM-5 (25) were higher than other catalysts.

Table 4 – Acidic properties of Cu-ZSM-5 catalysts.

Sample	C(L) (mmol/g)	C(B) (mmol/g)	Total acidity (mmol/g)	C(B)/C(L)
Cu-ZSM-5 (25)	0.83	0.34	1.17	0.41
Cu-ZSM-5 (50)	0.91	0.18	1.09	0.20
Cu-ZSM-5 (100)	0.49	0.03	0.52	0.06
Cu-ZSM-5 (200)	0.89	/	0.89	/

The specific C(L) and C(B) calculation formulas are in Appendix A. Supplementary data.
C(B): concentration of Brønsted acid sites; C(L): concentration of Lewis acid sites.

2.5.2. *Pyridine FTIR spectra*

The pyridine FTIR spectra with desorption temperatures of 100, 200, 300 and 400°C are presented in Fig. 10, and the acidic properties are outlined in Table 4. All samples revealed three bands owing to different acidity. The characteristic IR peak at 1545 cm^{-1} was attributed to the pyridine bonded to Brønsted acidity as pyridinium ions, and the vibration band at 1450 cm^{-1} is assigned to Lewis acidity. Additionally, the band at 1490 cm^{-1} could be ascribed to both Brønsted and Lewis acidity (Moreno-Recio et al., 2016; Pighin et al., 2018).

The quantitative analysis of Brønsted and Lewis acidity are determined by the vibration bands of 1450 and 1545 cm^{-1}, and the concentration of Brønsted and Lewis acid sites (C(B) and C(L)) was calculated by pyridine desorption at 100°C (Table 4) (Weng et al., 2017). The total acidity of these samples decreased in the order: Cu-ZSM-5 (25) > Cu-ZSM-5 (50) > Cu-ZSM-5 (200) > Cu-ZSM-5 (100), which is in accordance with the results of NH_3-TPD (Appendix A Fig. S1). The total acidity of Cu-ZSM-5 (200) was greater than Cu-ZSM-5 (100), which was assigned to the strong Lewis acidity. Interestingly, the C(B)/C(L)

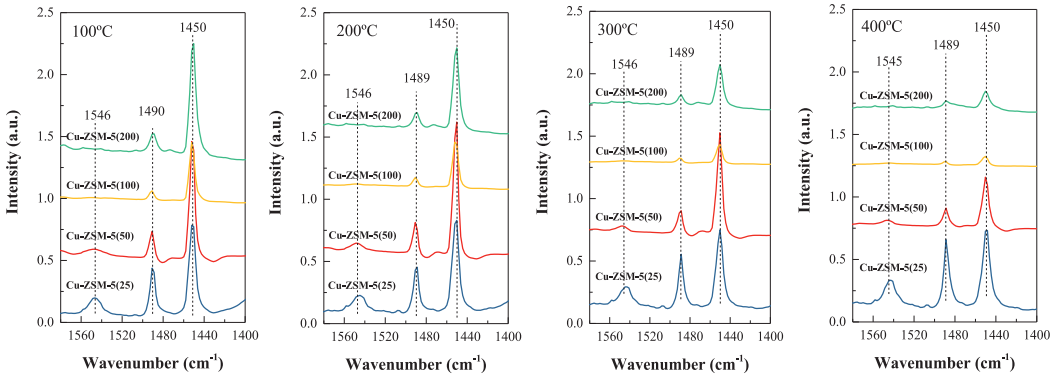

Fig. 10 – Pyridine Fourier transform infrared (FTIR) spectra of Cu-ZSM-5 catalysts with different SiO_2/Al_2O_3 ratios after desorption at 100, 200, 300, and 400°C.

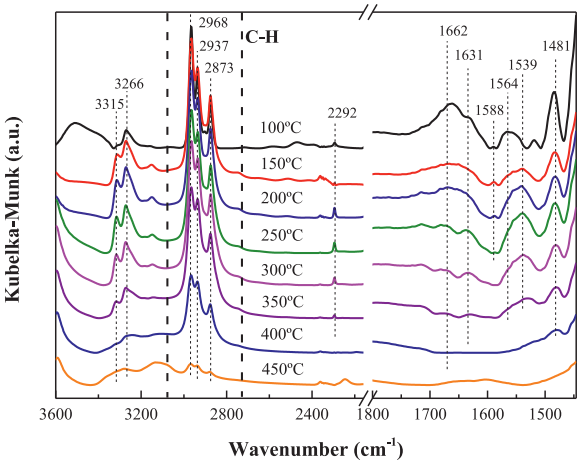

Fig. 11 – *In situ* diffuse reflectance infrared Fourier transform spectra (DRIFTs) of Cu-ZSM-5(25) in the flow of *n*-butylamine and O_2.

values decreased as the increase of the proportion of SiO_2 and Al_2O_3, which indicated that the Brønsted acid sites of catalysts with high SiO_2/Al_2O_3 ratio were much less than the catalyst with low SiO_2/Al_2O_3 ratio. For Cu-ZSM-5 (200), there were almost no Brønsted acid sites.

The results of pyridine FTIR and the acidic properties of Brønsted and Lewis acidity of pure ZSM-5 support are summarized in Appendix A Fig. S2 and Table S1. Comparing the corresponding supports, the Lewis and Brønsted acidity over Cu-loaded zeolite samples increased significantly after copper loading. The acid sites of ZSM-5 could be adjusted by the interactions of Cu with framework Al and non-framework Al in the supports (Blasco et al., 2007; Wang et al., 2015). Moreover, we believe that the acidity of the supports impacted the distribution of Cu species. The Brønsted acid sites and isolated Cu^{2+} species of Cu-ZSM-5 (25) catalyst were more than those of other samples. Analyses were conducted on the data of catalytic performance, the N_2 selectivity decreased in the order of Cu-ZSM-5 (25) > Cu-ZSM-5 (50) > Cu-ZSM-5 (100) > Cu-ZSM-5 (200), in agreement with the decreased order of C(B)/C(L) values. This result indicated that the acid site, especially Brønsted acidity of the Cu-loaded zeolite samples could impact the N_2 selectivity.

2.6. *In situ* DRIFTs

In situ diffuse reflectance infrared Fourier transform spectra (DRIFTs) is an important characterization method that is commonly applied to determine the possible intermediate species and reaction mechanism. Fig. 11 displays the DRIFT spectra of Cu-ZSM-5 (25) under *n*-butylamine and O_2. The bands at 2968, 2937, 2873 and 1481 cm^{-1} are attributed to the asymmetric (as) and symmetrical (s) vibrations of carbon hydrogen bonds (ν(as)CH_3, ν(as)CH_2, νs)CH_3 and δ(as)CH_3) of *n*-butylamine. The bands at 3315, 3266 and 1588 cm^{-1} were also detected and ascribed to the NH_2 functional groups (ν(s)NH_2, 2δNH_2, δNH_2) of *n*-butylamine (Ramis and Busca, 1983). With the increase in temperature, the vibrations of the C-H bond gradually decreased as well as the characteristic bands of the NH_2 functional group. The band of δNH_2 (1588 cm^{-1}) disappeared at 250°C. Simultaneously, two bands at 1539 and 1662 cm^{-1} appeared, corresponding to amide species (Ma et al., 2020; Zhang et al., 2016b). Furthermore, the bands at 1564 and 1631 cm^{-1} were attributed to the carboxylic acid and acetate species, which were further oxidized to produce final products (Zhang et al., 2016b). The band at 2292 cm^{-1} was also observed and attributed to the existence of CO_2 (Ma et al., 2018a). Based on the above results, *n*-butylamine catalytic oxidation on Cu-ZSM-5(25) sample begins with oxidation of *n*-butylamine to amide, which is further oxidized to produce intermediate products (carboxylic acid and acetate species) and to ultimately form CO_2 and H_2O. Additionally, N_2 and NO are generated from the oxidation of NH_2 species.

3. Conclusions

A series of Cu-loaded zeolite samples with SiO_2/Al_2O_3 ratios of 25, 50, 100, and 200 were synthesized and studied for *n*-butylamine catalytic degradation. All the catalysts showed well *n*-butylamine conversion, and the chemisorbed oxygen species and redox properties are the critical factors for the *n*-butylamine conversion. Notably, N_2 selectivity decreased with increasing SiO_2/Al_2O_3 ratio, and Cu-ZSM-5 (25) exhibited the highest N_2 selectivity among all samples, exceeding 95% at 400–450°C. According to characterization of these catalysts, Cu species mainly existed in the Cu^{2+} form on the catalysts, and isolated Cu^{2+} existed in tetragonally distorted octahedral coordination forms. With the increase in SiO_2/Al_2O_3 ratio, isolated Cu^{2+} gradually decreased, and the oligomeric Cu^{2+}-O^{2-}-Cu^{2+} species increased. Additionally, Brønsted acid sites play a crucial role in the catalytic degradation of *n*-butylamine. The

C(B)/C(L) values decreased in the order of Cu-ZSM-5 (25) > Cu-ZSM-5 (50) > Cu-ZSM-5 (100) > Cu-ZSM-5 (200). Thus, both isolated Cu^{2+} species and Brønsted acidity have important effects on the generation of N_2. Moreover, the SiO_2/Al_2O_3 ratio of zeolites could influence the Brønsted acid sites, which further affect the state and distribution of Cu species. The catalysts reported in this work could offer guiding significance for practical application of catalytic degradation of NVOCs.

Declaration of competing interest

The authors declare that they have no known competing financial interests or personal relationships that could have appeared to influence the work reported in this paper.

Acknowledgments

This work was supported by the National Natural Science Foundation of China (Nos. 21477149, 21677160, and 21707152) and Beijing Municipal Science and Technology Commission (Nos. Z181100000118003 and Z181100005418011).

Appendix A. Supplementary data

Supplementary material associated with this article can be found in the online version at doi:10.1016/j.jes.2020.03.015.

REFERENCES

Blasco, T., Boronat, M., Concepción, P., Corma, A., Law, D., Vidal-Moya, J.A., 2007. Carbonylation of methanol on metal-acid zeolites: evidence for a mechanism involving a multisite active center. Angew. Chem. Int. Ed. 46, 3938 –3841.
Das, S.K., Mukherjee, S., Lopes, L.M.F., Ilharco, L.M., Ferraria, A.M., Rego, A.M.B., et al., 2012. Synthesis, characterization and heterogeneous catalytic application of copper integrated mesoporous matrices. Dalton Trans. 43, 3215–3226.
Everaert, K., Baeyens, J., 2004. Catalytic combustion of volatile organic compounds. J. Hazard. Mater. B109, 113–139.
Feng, X., Tian, M., He, C., Li, L., Shi, J., Yu, Y., et al., 2020a. Yolk-shell-like mesoporous $CoCrO_x$ with superior activity and chlorine resistance in dichloromethane destruction. Appl. Catal. B-Environ. 264, 118493.
Feng, X., Chen, C., He, C., Chai, S., Yu, Y., Cheng, J., 2020b. Non-thermal plasma coupled with MOF-74 derived Mn-Co-Ni-O porous composite oxide for toluene efficient degradation. J. Hazard. Mater. 383, 121143.
Guieysse, B., Hort, C., Platel, V., Munoz, R., Ondarts, M., Revah, S., 2008. Biological treatment of indoor air for VOC removal: potential and challenges. Biotechnol. Adv. 26, 398–410.
Huang, Q., Zuo, S., Zhou, R., 2010. Catalytic performance of pillared interlayered clays (PILCs) supported CrCe catalysts for deep oxidation of nitrogen-containing VOCs. Appl. Catal. B-Environ. 95, 327–334.
Huang, B., Lei, C., Wei, C., Zeng, G., 2014. Chlorinated volatile organic compounds (Cl-VOCs) in environment sources, potential human health impacts, and current remediation technologies. Environ. Int. 71, 118–138.
He, C., Cheng, J., Zhang, X., Douthwaite, M., Pattisson, S., Hao, Z.P., 2019. Recent advances in the catalytic oxidation of volatile organic compounds: A review based on pollutant sorts and sources. Chem. Rev. 119, 4471–4568.
Jian, Y., Yu, T., Jiang, Z., Yu, Y., Douthwaite, M., Liu, J., et al., 2019. In-depth understanding of the morphology effect of α-Fe_2O_3 on catalytic ethane destruction. ACS Appl. Mater. Interfaces 11, 11369–11383.
Jiang, Z., He, C., Dummer, N.F., Shi, J., Tian, M., Ma, C., et al., 2018. Insight into the efficient oxidation of methyl-ethyl-ketone over hierarchically micro-mesostructured Pt/K-(Al)SiO_2 nanorod catalysts: Structure-activity relationships and mechanism. Appl. Catal. B-Environ. 226, 220–233.
Jiang, Z., Feng, X, Deng, J., He, C., Douthwaite, M., Yu, Y., et al., 2019. Atomic-scale insights into the low-temperature oxidation of methanol over a single-atom Pt1-Co_3O_4 catalyst. Adv. Funct. Mater. 29, 1902041.
Lai, S., Meng, D., Zhan, W., Guo, Y., Guo, Y., Zhang, Z., et al., 2015. The promotional role of Ce in Cu/ZSM-5 and *in situ* surface reaction for selective catalytic reduction of NO_x with NH_3. RSC Adv. 5, 90235–90244.
Li, W., Wang, J., Gong, H., 2009. Catalytic combustion of VOCs on non-noble metal catalysts. Catal. Today 148, 81–87.
Lian, Z., Liu, F., He, H., Shi, X., Mo, J., Wu, Z., 2014. Manganese-niobium mixed oxide catalyst for the selective catalytic reduction of NO_x with NH_3 at low temperatures. Chem. Eng. J. 250, 390–398.
Liotta, L.F., 2010. Catalytic oxidation of volatile organic compounds on supported noble metals. Appl. Catal. B-Environ. 100, 403–412.
Liu, Y., Deng, J., Xie, S., Wang, Z., Dai, H., 2016a. Catalytic removal of volatile organic compounds using ordered porous transition metal oxide and supported noble metal catalysts. Chin. J. Catal. 37, 1193–1205.
Liu, X., Wu, X., Weng, D., Shi, L., 2016b. Modification of Cu/ZSM-5 catalyst with CeO_2 for selective catalytic reduction of NO_x with ammonia. J. Rare Earth 34, 1004–1009.
Moreno-Recio, M., Santamaría-González, J., Maireles-Torres, P., 2016. Brönsted and Lewis acid ZSM-5 zeolites for the catalytic dehydration of glucose into 5-hydroxymethylfurfural. Chem. Eng. J. 303, 22–30.
Ma, M., Huang, H., Chen, C., Zhu, Q., Yue, L., Albilali, R., et al., 2018a. Highly active SBA-15-confined Pd catalyst with short rod-like micro-mesoporous hybrid nanostructure for n-butylamine low-temperature destruction. Mol. Catal. 455, 192–203.
Ma, Z., Ma, X., Ni, Y., Liu, H., Zhu, W., Guo, X., et al., 2018b. HZSM-35 zeolite catalyzed aldol condensation reaction to prepare acrylic acid and its ester: Effect of its acidic property. Chin. J. Catal. 39, 1762–1769.
Ma, M., Jian, Y., Chen, C., He, C., 2020. Spherical-like Pd/SiO_2 catalysts for n-butylamine efficient combustion: Effect of support property and preparation method. Catal. Today 339, 181–191.
Nanba, T., Masukawa, S., Uchisawa, J., Obuchi, A., 2004. Screening of catalysts for acrylonitrile decomposition. Catal. Lett. 93, 195–201.
Nanba, T., Masukawa, S., Ogata, A., Uchisawa, J., Obuchi, A., 2005. Active sites of Cu-ZSM-5 for the decomposition of acrylonitrile. Appl. Catal. B-Environ. 61, 288–296.
Nanba, T., Masukawa, S., Uchisawa, J., Obuchi, A., 2007. Mechanism of acrylonitrile decomposition over Cu-ZSM-5. J. Mol. Catal. A-Chem. 276, 130–136.
Nanba, T., Masukawa, S., Uchisawa, J., Obuchi, A., 2008. Effect of support materials on Ag catalysts used for acrylonitrile decomposition. J. Catal. 259, 250–259.
Navlani-García, M., Martis, M., Lozano-Castelló, D., Cazorla-Amorós, D., Mori, K., Yamashita, H., 2015. Investigation of Pd nanoparticles supported on zeolites for hydrogen production from formic acid dehydrogenation. Catal. Sci. Technol. 5, 364–371.
Praliaud, H., Mikhailenko, S., Chajar, Z., Primet, M., 1998. Surface and bulk properties of Cu-ZSM-5 and Cu/Al_2O_3 solids during redox treatments. Correlation with the selective reduction of nitric oxide by hydrocarbons. Appl. Catal. B-Environ. 16, 359–374.
Parmar, G.R., Rao, N.N., 2008. Emerging control technologies for volatile organic compounds. Crit. Rev. Env. Sci. Tec. 39, 41–78.
Pereda-Ayo, B., Torre, U.D.L., Illán-Gómez, M.J., Bueno-López, A., González-Velasco, J.R., 2014. Role of the different copper species on the activity of Cu/zeolite catalysts for SCR of NO_x with NH_3. Appl. Catal. B-Environ. 147, 420–428.
Pighin, E.A., Cosimo, J.I.Di, Díez, V.K., 2018. Kinetic and mechanistic study of triose sugar conversion on Lewis and Brønsted acid solids. Mol. Catal. 458, 189–197.
Ramis, G., Busca, G., 1983. FTIR spectra of adsorbed n-butylamine. J. Mol. Struct. 193, 93–100.
Rutkowska, M., Pacia, I., Basąg, S., Kowalczyk, A., Piwowarska, Z., Duda, M., et al., 2017. Catalytic performance of commercial Cu-ZSM-5 zeolite modified by desilication in NH_3-SCR and NH_3-SCO processes. Micropor. Mesopor. Mat. 246, 193–206.
Scirè, S., Liotta, L.F., 2012. Supported gold catalysts for the total oxidation of volatile organic compounds. Appl. Catal. B-Environ. 125, 222–246.
Sun, P., Guo, R., Liu, S., Wang, S., Pan, W., Li, M., 2017. The enhanced performance of MnO_x catalyst for NH_3-SCR reaction by the modification with Eu. Appl. Catal. A-Gen. 531, 129–138.
Tian, M., Guo, X., Dong, R., Guo, Z., Shi, J., Yu, Y., et al., 2019. Insight into the boosted catalytic performance and chlorine resistance of nanosphere-like meso-macroporous $CrO_x/MnCo_3O_x$ for 1, 2-dichloroethane destruction. Appl. Catal. B-Environ. 259, 118018.
Wang, S., Guo, W., Zhu, L., Wang, H., Qiu, K., Cen, K., 2015. Methyl acetate synthesis from dimethyl ether carbonylation over mordenite modified by cation exchange. J. Phys. Chem. C 119, 524–533.
Weng, X., Sun, P., Long, Y., Meng, Q., Wu, Z., 2017. Catalytic oxidation of chlorobenzene over $Mn_xCe_{1-x}O_2$/HZSM-5 catalysts: a study with practical implications. Environ. Sci. Technol. 51, 8057–8066.
Xue, H., Guo, X., Wang, S., Sun, C., Yu, J., Mao, D., 2018. Poisoning effect of CaO on Cu/ZSM-5 for the selective catalytic reduction of NO with NH_3. Catal. Commun. 112, 53–57.
Xing, X., Li, N., Cheng, J., Sun, Y., Wang, G., Zhang, Z., et al., 2019. Hydrotalcite-derived $Cu_xMg_{3-x}AlO$ oxides for catalytic degradation of n-butylamine with low concentration NO and pollutant destruction mechanism. Ind. Eng. Chem. Res. 58, 9362–9371.
Xing, X., Li, N., Sun, Y., Wang, G., Cheng, J., Hao, Z., 2020. Selective catalytic oxidation of n-butylamine over Cu-zeolite catalysts. Catal. Today 339, 192–199.
Yashnik, S.A., Ismagilov, Z.R., Anufrienko, V.F., 2005. Catalytic properties and electronic structure of copper ions in Cu-ZSM-5. Catal. Today 110, 310–322.
Yashnik, S.A., Salnikov, A.V., Vasenin, N.T., Anufrienko, V.F., Ismagilov, Z.R., 2012. Regulation of the copper-oxide cluster structure and DeNO_x activity of Cu-ZSM-5 catalysts by variation of OH/Cu^{2+}. Catal. Today 197, 214–227.
Zhang, R., Liu, N., Lei, Z., Chen, B., 2016a. Selective transformation of various nitrogen-containing exhaust gases toward N_2 over zeolite catalysts. Chem. Rev. 116, 3658–3721.
Zhang, R., Li, P., Xiao, R., Liu, N., Chen, B., 2016b. Insight into the mechanism of catalytic combustion of acrylonitrile over Cu-doped perovskites by an experimental and theoretical study. Appl. Catal. B: Environ. 196, 142–154.